RSC Advances

PAPER

View Article Online
View Journal | View Issue

Cite this: *RSC Adv.*, 2017, **7**, 10618

Mechanochemically induced transformation of CoO(OH) into Co_3O_4 nanoparticles and their highly reversible Li storage characteristics†

Jae-Wan Park and Cheol-Min Park*

Received 31st October 2016
Accepted 3rd February 2017

DOI: 10.1039/c6ra26099c

rsc.li/rsc-advances

A simple synthetic method for the mechanochemically induced transformation of cobalt oxyhydroxides (CoO(OH)) into cobalt oxide (Co_3O_4) nanoparticles is developed. Using this method, extremely small and well-dispersed Co_3O_4 (3–5 nm) nanoparticles are synthesized and their use as a high-performance anode for Li-ion batteries is evaluated. The Co_3O_4 nanoparticle electrode shows excellent electrochemical performances such as a highly reversible capacity of 1023 mA h g^{-1} with excellent cycling behavior over 100 cycles and a superior rate capability of 760 mA h g^{-1} at an extremely fast current rate of 3C. This simple mechanochemically induced transformation method for extremely small and well-dispersed cobalt oxide nanoparticles is highly applicable to the preparation of other metal oxide nanoparticles for obtaining highly reversible Li storage characteristics.

Introduction

Rechargeable Li-ion batteries have important applications as alternative green energy-storage systems for high-tech electronic mobile devices and electric vehicles. Graphite is a common anode material for Li-ion batteries owing to its relatively low cost and stable cycling performance; however, it has a limited theoretical capacity of 372 mA h g^{-1} and poor rate capability.[1–5] Therefore, alternative anode materials with large capacities and fast rate capabilities are required for the realization of zero-emission and next-generation energy storage systems.

As an alternative, transition metal oxides (M_xO_y, where M represents Fe, Co, Ni, Mo, *etc.*) have been suggested as high-capacity anode materials.[6–21] M_xO_y electrodes show high capacities and undergo interesting conversion/recombination reactions during Li insertion/extraction, which involve the formation of Li_2O and metal by a conversion reaction during Li insertion and a recombination reaction to give M_xO_y during Li extraction. However, to achieve good electrochemical performance, including high capacity, fast rate capability, and long cycling behavior, nanostructured transition metal oxides are required.[6–22] Nano-sized materials can undergo highly reversible recombination reactions with Li by maximizing their reactivity with Li, minimizing the volume change during Li reactions, and providing short Li-ion diffusion paths. However, nanostructured metal oxides are generally synthesized by complicated chemical methods, such as co-precipitation, reduction, and sol–gel processes, which result in poor initial coulombic efficiencies due to the presence of residual salts or impurities formed during the synthesis. Thus, the preparation of nanostructured metal oxides using a simple solid-state method without any chemical solvents or salts would provide a breakthrough in the realization of high-performance metal oxide-based anodes. Among the various solid-state synthetic methods available, the high-energy ball milling (HEBM) technique is promising because no impurities are produced during this process, which is an extremely simple compared with chemical synthetic methods. The HEBM technique has been applied to the preparation of amorphized Sn/Co/C composites as a commercial anode material in the Nexelion battery developed by Sony in 2005.[23] However, despite the advantageous features of the HEBM technique, it has not been widely applied to the synthesis of nanostructured metal oxides because the high energy generated during the HEBM process affects the mechanical properties of conventional ceramics, resulting in broken structures or agglomerated particles.[24]

Transition metal oxyhydroxides (MO(OH), where M represents a transition metal) have been investigated widely for electrocatalytic applications.[25,26] Additionally, MO(OH) materials undergo interesting thermal conversion reactions, which are thermodynamically driven, to form metal oxides (M_3O_4, where M represents a transition metal), as shown in eqn (1).[27–30]

$$12MO(OH) \rightarrow 4M_3O_4 + 6H_2O\uparrow + O_2\uparrow \quad (1)$$

For instance, CoO(OH) is transformed into water vapor, oxygen gas, and Co_3O_4 in the temperature range of 264–391 °C

School of Materials Science and Engineering, Kumoh National Institute of Technology, Gumi, Gyeongbuk 39177, Republic of Korea. E-mail: cmpark@kumoh.ac.kr; Fax: +82-54-478-7769; Tel: +82-54-478-7746

† Electronic supplementary information (ESI) available: Experimental procedures, characterization and electrochemical data of the compound. See DOI: 10.1039/c6ra26099c

under an air atmosphere.[27] Similar thermal transformation reactions have also been observed for other MO(OH), such as FeO(OH), MnO(OH), and TiO(OH).[28–30]

Among the various transition metal oxides, cobalt oxides (Co_3O_4 or CoO) have been widely investigated as electrode materials for Li-ion batteries owing to its facile preparation by various conventional synthesis routes, such as molten-salt method, urea combustion method, hydrothermal method, precipitation, template method, virus-enabled synthesis, ammonia-evaporation-induced method, thermal decomposition, *etc.*[9,31–39]

In this study, we synthesized Co_3O_4 nanoparticles by a simple HEBM method, using the thermodynamically induced conversion reaction of CoO(OH). The mechanochemically transformed Co_3O_4 nanoparticles were evaluated for use as high-performance anodes for rechargeable Li-ion batteries.

Experimental

Samples preparation

Co_3O_4 nanoparticles were synthesized by a simple HEBM process. CoO(OH) (Samchun Pure Chemical, 99%, average size: *ca.* 5 μm) powder of 5 g was placed in a hardened-steel vial with a volume of 80 cm^3 along with stainless-steel balls (diameter: 3/8 in. and 3/16 in.) at a ball-to-powder ratio of 20 : 1 by weight. The vial was assembled in an Ar-filled glove box, and the CoO(OH) powder was subjected to HEBM (Spex-8000) under an Ar atmosphere for 12 h.

Materials characterization

The synthesized Co_3O_4 nanoparticles were characterized using X-ray diffraction (XRD, DMAX2500-PC, Rigaku), high-resolution transmission electron microscopy (HRTEM, FEI F20, operating at 200 kV), and energy-dispersive spectroscopy (EDS) attached to the HRTEM. Brunauer–Emmett–Teller (BET, 3Flex) surface area was analyzed by the nitrogen-adsorption isotherm of the Co_3O_4 nanoparticles sample. To observe the structural changes occurring in the active materials of the nanoparticle electrodes during Li insertion/extraction, *ex situ* XRD and extended absorption fine structure (EXAFS) analyses were conducted. For the *ex situ* analyses, the electrodes at the selected potentials were detached from the cells in an Ar-filled glove box and coated with polyimide tape (Kapton), which served as a protective film. The Co K-edge EXAFS spectra for the synthesized Co_3O_4 nanoparticles electrode were recorded at the 8C (Nano XAFS) beamline in the 3.0 GeV storage ring at the Pohang Light Source (PLS), South Korea.

Electrochemical measurements

For the electrochemical evaluation of the synthesized Co_3O_4 samples, the electrodes were prepared by coating a slurry on Cu foil substrates. The slurry consisted of the Co_3O_4 (80 wt%) active material, carbon black (Denka, 10 wt%) conducting agent, and polyvinylidene fluoride (10 wt%) binder dissolved in *N*-methyl-2-pyrrolidone. Each mixture samples were vacuum-dried at 120 °C for 3 h and then pressed using roll press. The synthesized Co_3O_4 electrode had a loading of *ca.* 3.5 mg cm^{-2}. Electrochemical coin-type cells were assembled in an high purity Ar-filled glove box using Celgard 2400 separator, Li foil counter and reference electrodes, and 1 M $LiPF_6$ in ethylene carbonate/diethyl carbonate (EC/DEC, 1 : 1 v/v, Panax Starlyte) electrolyte. To investigate the electrochemical reaction resistance of the electrodes, electrochemical impedance spectroscopy (EIS) was conducted using an impedance analyzer (ZIVE MP2A, WonATech), and the results were recorded (amplitude: 5 mV, frequency range: 10^5 to 10^{-2} Hz). Cyclic voltammogram (CV) was measured in the range of 0.0–3.0 V at a scanning rate of 0.05 mV s^{-1} using a SP-240 potentiostat (Bio-Logic). With the exception of the rate-capability tests, all cells were tested galvanostatically between 0.0 and 3.0 V (*vs.* Li^+/Li) at a current density of 100 mA g^{-1} using a Maccor automated tester, in which Li was inserted into the electrode on discharging and extracted from the working electrode on charging.

Results and discussion

The X-ray diffraction (XRD) pattern of commercially available monoclinic CoO(OH) is shown in Fig. 1a. Considering the

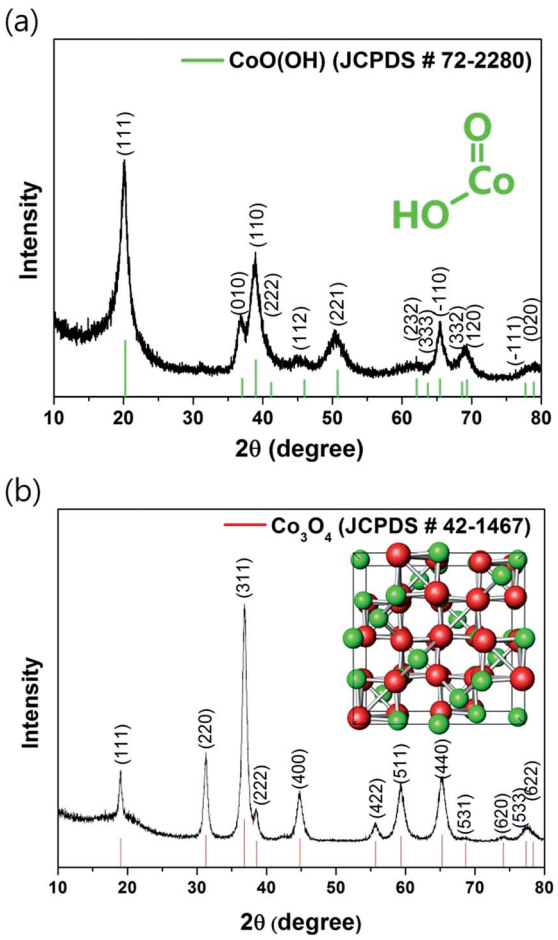

Fig. 1 Synthesis of Co_3O_4 nanoparticles. XRD patterns of (a) commercially available CoO(OH) powder and (b) Co_3O_4 obtained by mechanochemical transformation of CoO(OH) powder. The crystalline structure of Co_3O_4 is also shown as inset in (b).

thermodynamic conversion reaction (1) of the transition metal oxyhydroxides into their oxides, CoO(OH) was subjected to HEBM processing for 12 h. As confirmed in Fig. 1b, the HEBM technique completely transformed CoO(OH) into the Co_3O_4 (JCPDS #42-1467). The synthesized Co_3O_4 has the cubic crystalline structure (space group: $Fd\bar{3}mZ$, $a = 8.0835$ Å), which has three-dimensional tetragonal channels along each axis. These interesting tetragonal channels of Co_3O_4 enable facile Li storage and diffusion. The mechanochemically induced transformation of the CoO(OH) into Co_3O_4 was caused by the high energy (temperature > 200 °C and pressure of ~6 GPa) generated within the vial during the HEBM process.[24]

To clarify in detail the structure and morphology of the synthesized Co_3O_4, HRTEM analysis was performed. The TEM bright-field and HRTEM micrographs with their corresponding selected area electron diffraction (SAED) and Fourier transform (FT) patterns for the synthesized Co_3O_4 nanoparticles are shown in Fig. 2a–c. In Fig. 2a, the bright-field TEM micrograph indicates the presence of nano-sized Co_3O_4 particles. The HRTEM image (Fig. 2b) and its corresponding SAED and FT patterns (Fig. 2c) demonstrate the even dispersion of Co_3O_4 nanoparticles that are approximately 3–5 nm in size. Additionally, all *d*-spacings derived from the SAED and FT patterns exactly corresponded to the Co_3O_4 phase, which confirms that the nanoparticles contain no impurities. The O_2 and H_2O gases generated during the HEBM process might act as grinding and controlling agents to prevent agglomeration, which results in well-dispersed metal oxide nanoparticles. These results confirm that the HEBM process is a very advantageous and useful technique for synthesizing well-dispersed transition metal oxide nanoparticles with extremely small sizes using transition metal oxyhydroxides.

To evaluate the electrochemical performance of the synthesized Co_3O_4 nanoparticles for use as an anode material for rechargeable lithium-ion batteries, the electrochemical property was investigated. The voltage profile of the Co_3O_4 nanoparticles electrode is displayed in Fig. 3. The Co_3O_4 nanoparticles electrode showed high initial discharge and charge capacities of 1205 and 855 mA h g^{-1}, respectively. The discharge (Li insertion) capacity of the electrode was much higher than its theoretical capacity of 890 mA h g^{-1}, which was attributed to irreversible Li reactions associated with the irreversible formation of a solid electrolyte interphase (SEI) on the surface of Co_3O_4, kinetic limitations of electrochemical reaction, partial reduction of the electrolyte solvent, and interfacial storage.[3,40–43] However, the charge (Li extraction) capacity of the electrode was similar to the theoretical capacity, which demonstrates that the electrode undergoes a highly reversible reaction with Li.

The electrochemical impedance results of the CoO(OH) and synthesized Co_3O_4 electrodes were plotted and compared in Fig. 4. The Co_3O_4 nanoparticles electrode showed a smaller semicircle than CoO(OH), confirming the higher electrical conductivity in the Co_3O_4 nanoparticles electrode. The smaller electrochemical reaction resistance in the Co_3O_4 nanoparticles electrode was attributed to the mechanochemically induced transformation of CoO(OH) into Co_3O_4 nanoparticles with well-dispersed and extremely small sizes. The nitrogen-adsorption isotherm of the Co_3O_4 nanoparticles, which had a BET surface area of 85.33 m^2 g^{-1}, which also supports the well-dispersed and extremely small sized Co_3O_4 nanoparticles.

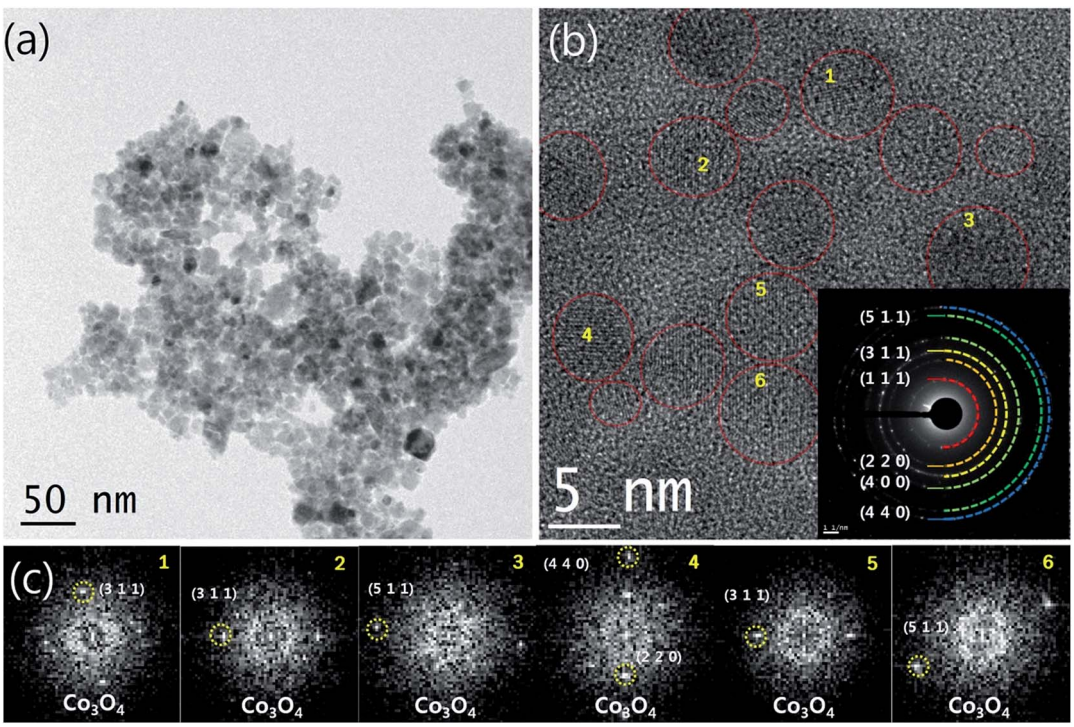

Fig. 2 Morphological investigation of Co_3O_4 nanoparticles. (a) TEM bright-field and (b) HRTEM images with their corresponding SAED and (c) FT patterns for synthesized Co_3O_4 nanoparticles.

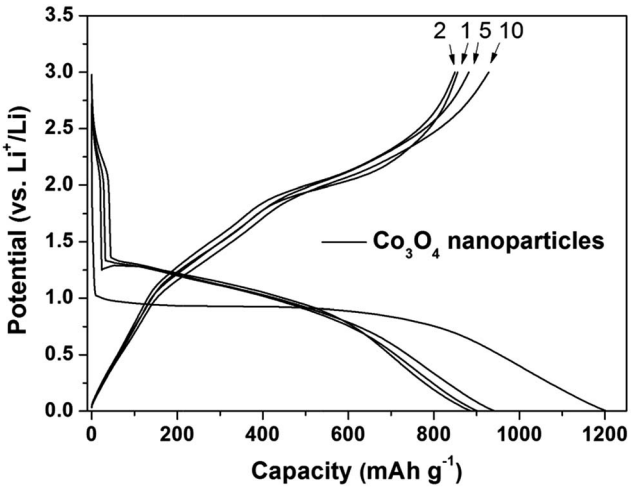

Fig. 3 Electrochemical performance of Co_3O_4 nanoparticles electrode. Galvanostatic voltage profile of Co_3O_4 nanoparticles electrode (current density: 100 mA g^{-1}, voltage window: 0.0–3.0 V).

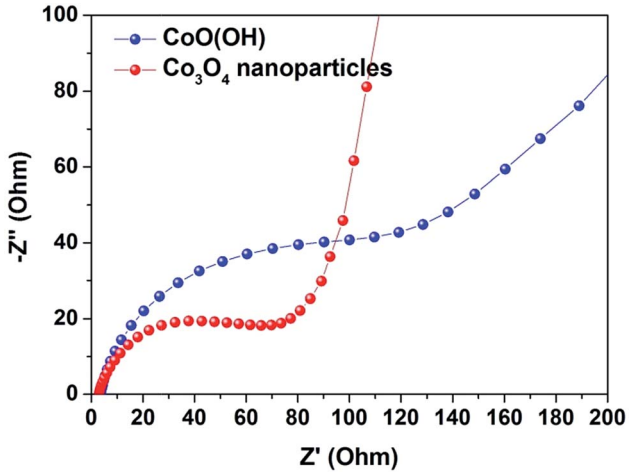

Fig. 4 Electrochemical impedance of Co_3O_4 nanoparticles electrode. Electrochemical Nyquist plots of CoO(OH) and Co_3O_4 nanoparticles electrodes.

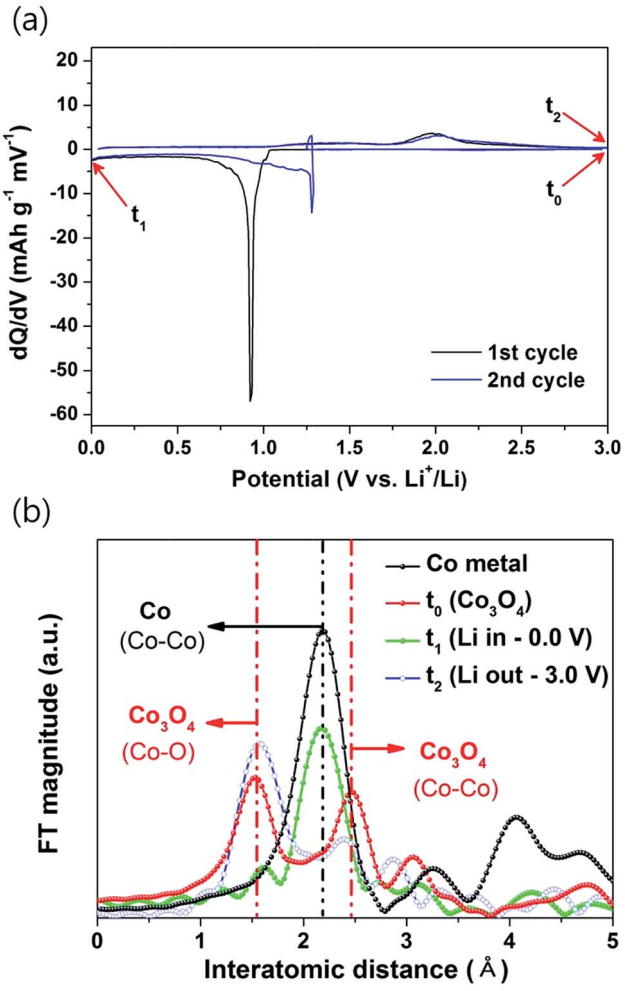

Fig. 5 Electrochemical reaction mechanism of Co_3O_4 nanoparticles electrode. (a) DCP for the first and second cycling and (b) Co K-edge EXAFS results during the first cycle for Co_3O_4 nanoparticles electrode.

Fig. 5a and S1 in ESI† show the differential capacity plots (DCP) and CV results for the first and second cycles of the Co_3O_4 nanoparticles electrode, respectively. The DCP of the Co_3O_4 nanoparticles electrode showed a large peak at approximately 0.9 V during discharging and a broad peak at approximately 2.0 V during charging (Fig. 5a), which coincided well with the CV results (Fig. S1†). The DCP and CV results demonstrate that the Co_3O_4 nanoparticles electrode underwent one-step electrochemical reaction with Li during discharging and charging.

To elucidate the reaction mechanism of the Co_3O_4 nanoparticles electrode, *ex situ* XRD analyses (Fig. S2 in ESI†) were carried out at the selected potentials indicated in the DCP result (Fig. 5a). However, no distinctive phases were observed in the *ex situ* XRD spectra, which confirms that the electrodes were amorphized by reaction with Li. Therefore, to investigate the reaction mechanism in the amorphized electrode, Co K-edge EXAFS spectra were recorded for the synthesized Co_3O_4 nanoparticles electrode at the 8C (Nano XAFS) beamline in a storage ring of 3.0 GeV at the Pohang Light Source (PLS), South Korea. Fig. 5b shows the Fourier transformed *k*-weighted Co K-edge EXAFS spectrum of the Co_3O_4 nanoparticles electrode during the first cycle. The main peaks observed for the Co_3O_4 nanoparticles corresponded well the Co–O (~1.5 Å) and Co–Co (~2.5 Å) bonds of pristine Co_3O_4 (Fig. 5b-t_0).[44] In the fully discharged state at 0.0 V (Fig. 5b-t_1), the Co–O (~1.5 Å) and Co–Co (~2.5 Å) peaks disappeared, and the only the Co–Co (~2.2 Å) peak of Co metal was observed, which confirms that Co_3O_4 was transformed into Li_2O and Co by a conversion reaction during discharging. However, some recent studies demonstrated that intermediated $Li_xCo_3O_4$ phases can be formed at the low current densities during first Li insertion.[32,45,46] In contrast, when the electrode was in the fully charged state at 3.0 V (Fig. 5b-t_2), the Co–O (~1.5 Å) and Co–Co (~2.5 Å) peaks of Co_3O_4 clearly reappeared, which demonstrates the full recombination of Co_3O_4 nanoparticles during Li extraction. Therefore, on the basis of the EXAFS results, the Co_3O_4 nanoparticles

electrode underwent the following conversion/recombination reactions during discharging/charging, respectively.

$$\text{During discharging: } Co_3O_4 \rightarrow Li_xCo_3O_4 \rightarrow Co + Li_2O \quad (2)$$

$$\text{During charging: } Co + Li_2O \rightarrow Co_3O_4 \quad (3)$$

The conversion (2) and recombination (3) reactions during Li insertion and extraction in transition metal oxide-based electrodes are well known.[6–21,31–39] The Co_3O_4 nanoparticles synthesized by a mechanochemically induced conversion reaction showed full recombination reactions without any residual non-recombined Co metal, as confirmed by the EXAFS results, which contributed to their highly reversible reactions with Li.

Fig. 6a compares the cycling performances of the Co_3O_4 nanoparticles electrode and a mesocarbon microbead (MCMB) graphite electrode. The Co_3O_4 nanoparticles electrode showed high reversibility and very stable capacity retention with a high capacity of 1023 mA h g^{-1} over 100 cycles. These characteristics are much better than those of previously reported various nanostructured Co_3O_4 electrodes, such as nanocage, nanotube, mesoporous, needle-like, self-stacked nanosheet, and multishelled hollow sphere electrodes.[36,47–53] The excellent cycling performance of the Co_3O_4 nanoparticles electrode is attributed to the preparation of extremely small and well-dispersed Co_3O_4 nanoparticles, which allowed fully reversible conversion/recombination reactions during repeated discharging/charging and accommodated large volume changes of the active materials during repeated cycling. The rate capabilities of the Co_3O_4 nanoparticles electrode were evaluated as a function of the C rate, as shown in Fig. 6b and S3 in ESI,† in which *C* is defined as full use of the limited charging capacity, 900 mA h g^{-1}, in 1 h. The reversible capacities of the Co_3O_4 nanoparticles electrode at a high current rate of 3C were 760 mA h g^{-1} corresponding to *ca.* 86% of the initial charge capacities. The Co_3O_4 nanoparticles electrode showed better rate capabilities than the MCMB graphite electrode. This improved rate capability was ascribed to the short diffusion path obtained by the preparation of extremely small and well dispersed nanoparticles of Co_3O_4 (3–5 nm) by the mechanochemically induced transformation reaction, which leads to fast Li ion diffusion rates.

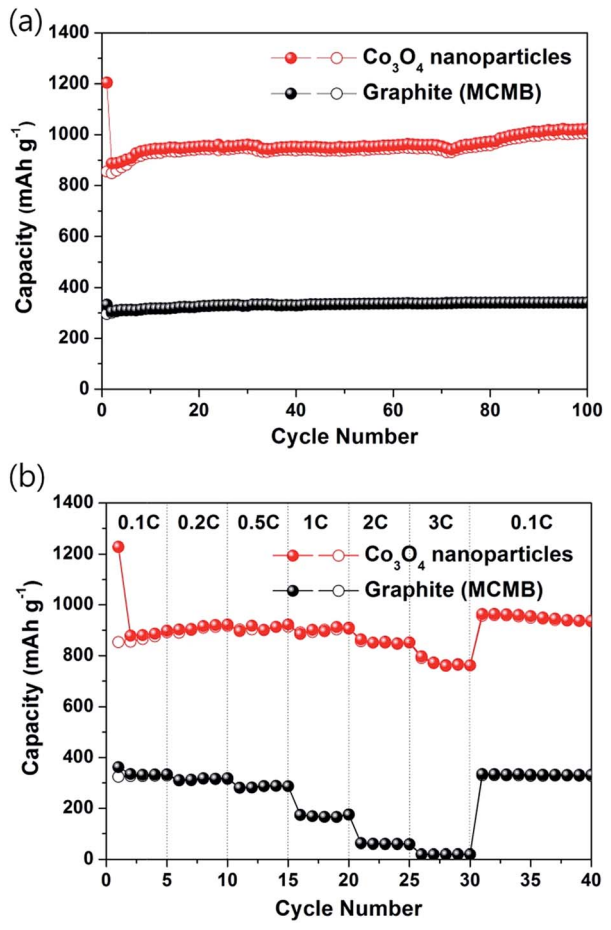

Fig. 6 Cycling performance and rate capability of Co_3O_4 nanoparticles electrode. (a) Cycling performance of the Co_3O_4 nanoparticles electrode and an MCMB-graphite electrode at a cycling rate of 100 mA g^{-1}, and (b) rate capabilities of the Co_3O_4 nanoparticles electrode and an MCMB-graphite electrode at various C rates.

Conclusions

In summary, we synthesized extremely small and well-dispersed Co_3O_4 (3–5 nm) nanoparticles by a simple mechanochemically induced transformation of the CoO(OH). The synthesized Co_3O_4 nanoparticles electrode showed highly reversible Li reactions, and their conversion and full recombination reactions during discharging and charging were clearly demonstrated using EXAFS analyses. The Co_3O_4 nanoparticles electrode showed excellent electrochemical performance with a highly reversible capacity of 1023 mA h g^{-1} over 100 cycles and a fast rate capability of 760 mA h g^{-1} at a high current rate of 3C. Based on these results, this mechanochemical synthetic method for extremely small and well-dispersed cobalt oxide nanoparticles is highly applicable to the preparation other oxide nanoparticles for obtaining high-performance electrode materials for rechargeable Li-ion batteries.

Acknowledgements

This paper was supported by Research Fund, Kumoh National Institute of Technology.

Notes and references

1 C.-M. Park, J.-H. Kim, H. Kim and H.-J. Sohn, *Chem. Soc. Rev.*, 2010, **39**, 3115.
2 R. Marom, S. F. Amalraj, N. Leifer, D. Jacob and D. J. Aurbach, *J. Mater. Chem.*, 2011, **21**, 9938.
3 J. Cabana, L. Monconduit, D. Larcher and M. R. Palacin, *Adv. Mater.*, 2010, **22**, E170.
4 D. Larcher, S. beattie, M. Morcrette, K. Edstrom, J.-C. Jumas and J.-M. Tarascon, *J. Mater. Chem.*, 2007, **17**, 3759.
5 V. Etacheri, R. Marom, R. Elazari, G. Salitra and D. Aurbach, *Energy Environ. Sci.*, 2011, **4**, 3243.
6 P. Poizot, S. Lauruelle, S. Grugeon, L. Dupont and J.-M. Tarascon, *Nature*, 2000, **407**, 496.

7 P. L. Taberna, S. Mitra, P. Poizot, P. Simon and J.-M. Tarascon, *Nat. Mater.*, 2006, **5**, 567.
8 Y.-S. Hu, Y.-G. Guo, W. Sigle, S. Hore, P. Balaya and J. Maier, *Nat. Mater.*, 2006, **5**, 713.
9 B.-C. Yu, J.-O. Lee, J. H. Song, C.-M. Park, C. K. Lee and H.-J. Sohn, *J. Solid State Electrochem.*, 2012, **16**, 2631.
10 M. V. Reddy, G. V. Subba Rao and B. V. R. Chowdari, *Chem. Rev.*, 2013, **113**, 5364.
11 H. Xia, W. Xiong, C. K. Lim, Q. Yao, Y. Wang and J. Xie, *Nano Res.*, 2014, **7**, 1797.
12 H. Xia, C. Hong, X. Shi, B. Li, G. Yuan, Q. Yao and J. Xie, *J. Mater. Chem. A*, 2015, **3**, 1216.
13 G. Ji, Q. Yao, B. Qu, D. Chen, W. Chen, J. Xie and J. Y. Lee, *NPG Asia Mater.*, 2016, **8**, e247.
14 Q. Xia, M. Xu, H. Xia and J. Xie, *ChemNanoMat*, 2016, **2**, 588; B. Das, M. V. Reddy and B. V. R. Chowdari, *J. Alloys Compd.*, 2013, **565**, 90.
15 M. V. Reddy, Y. Xu, V. Rajarajan, T. Ouyang and B. V. R. Chowdari, *ACS Sustainable Chem. Eng.*, 2015, **3**, 3035.
16 C. T. Cherian, M. V. Reddy, G. V. Subba Rao, C. H. Sow and B. V. R. Chowdari, *J. Solid State Electrochem.*, 2012, **16**, 1823.
17 M. V. Reddy, C. Y. Quan, K. W. Teo, L. J. Ho and B. V. R. Chowdari, *J. Phys. Chem. C*, 2015, **119**, 4709.
18 C. T. Cherian, J. Sundaramurthy, M. V. Reddy, P. S. Kumar, K. Mani, D. Pliszka, C. H. Sow, S. Ramakrishna and B. V. R. Chowdari, *ACS Appl. Mater. Interfaces*, 2013, **5**, 9957.
19 Y. Wu, R. Balakrishna, M. V. Reddy, A. S. Nair, B. V. R. Chowdari and S. Ramakrishna, *J. Alloys Compd.*, 2012, **517**, 69.
20 A. K. Ramasami, M. V. Reddy and B. V. R. Chowdari, *Mater. Sci. Semicond. Process.*, 2015, **40**, 194.
21 N. A. Chernova, M. Roppolo, A. C. Dillon and M. S. Whittingham, *J. Mater. Chem.*, 2009, **19**, 2526.
22 J. Cheng, B. Wang, C.-M. Park, Y. Wu, H. Huang and F. Nie, *Chem.–Eur. J.*, 2013, **19**, 9866.
23 H. Ishihara, S. Mizutani and H. Inoue, US 11/268,010, 2005.
24 C. Suryanarayana, *Prog. Mater. Sci.*, 2001, **46**, 1.
25 C. S. Lim, C. K. Chua, Z. Sofer, K. Klimova, C. Boothroyd and M. Pumera, *J. Mater. Chem. A*, 2015, **3**, 11920.
26 L. Liu, Z. Zhou and C. Peng, *Electrochim. Acta*, 2008, **54**, 434.
27 K. Przepiera and A. Przepiera, *J. Therm. Anal. Calorim.*, 2003, **74**, 659.
28 M. M. Najafpour, R. Mostafalu, M. Hołynska and F. Ebrahimi, *J. Photochem. Photobiol., B*, 2015, **152**, 112.
29 S. Music, S. Krehula and S. Popovic, *Mater. Lett.*, 2004, **58**, 444.
30 J. A. Lee, C. E. Newnham, F. S. Stone and F. L. Tye, *J. Solid State Chem.*, 1980, **31**, 81.
31 M. V. Reddy, Z. Beichen, K. P. Loh and B. V. R. Chowdari, *CrystEngComm*, 2013, **15**, 3568.
32 M. V. Reddy, Z. Beichen, L. J. Nicholette, Z. Kaimeng and B. V. R. Chowdari, *Electrochem. Solid-State Lett.*, 2011, **14**, A79.
33 M. V. Reddy, G. Prithivi, K. P. Loh and B. V. R. Chowdari, *ACS Appl. Mater. Interfaces*, 2014, **6**, 680.
34 H. Huang, W. J. Zhu, X. Y. Tao, Y. Xia, Z. Y. Yu, J. W. Fang, Y. P. Gan and W. K. Zhang, *ACS Appl. Mater. Interfaces*, 2012, **4**, 5974.
35 G. Binotto, D. Larcher, A. S. Prakash, R. H. Urbina, M. S. Hegde and J. M. Tarascon, *Chem. Mater.*, 2007, **19**, 3032.
36 W. Y. Li, L. N. Xu and J. Chen, *Adv. Funct. Mater.*, 2005, **15**, 851.
37 K. T. Nam, D. W. Kim, P. J. Yoo, C. Y. Chiang, N. Meethong, P. T. Hammond, Y. M. Chiang and A. M. Belcher, *Science*, 2006, **312**, 885.
38 Y. G. Li, B. Tan and Y. Y. Wu, *Nano Lett.*, 2008, **8**, 265.
39 R. Z. Yang, Z. X. Wang, J. Y. Liu and L. Q. Chen, *Electrochem. Solid-State Lett.*, 2004, **7**, A496.
40 P. Balaya, H. Li, L. Kienle and J. Maier, *Adv. Funct. Mater.*, 2003, **13**, 621.
41 M. V. Reddy, B. L. W. Wen, K. P. Loh and B. V. R. Chowdari, *ACS Appl. Mater. Interfaces*, 2013, **5**, 7777.
42 C. T. Cherian, M. Zheng, M. V. Reddy, B. V. R. Chowdari and C. H. Sow, *ACS Appl. Mater. Interfaces*, 2013, **5**, 6054.
43 M. V. Reddy, G. V. Subba Rao and B. V. R. Chowdari, *J. Mater. Chem.*, 2011, **21**, 10003.
44 D.-H. Ha, L. M. Moreau, S. Honrao, R. G. Hennig and R. D. Robinson, *J. Phys. Chem. C*, 2013, **117**, 14303.
45 S. Sun, X. Zhao, M. Yang, L. Wu, Z. Wen and X. Shen, *Sci. Rep.*, 2016, **6**, 19564.
46 Y. Wang, H. Xia, L. Lu and J. Lin, *ACS Nano*, 2010, **4**, 1425.
47 N. Yan, L. Hu, Y. Li, Y. Wang, H. Zhong, X. Hu, X. Kong and Q. Chen, *J. Phys. Chem. C*, 2012, **116**, 7227.
48 D. Su, X. Xie, P. Munroe, S. Dou and G. Wang, *Sci. Rep.*, 2014, **4**, 6519.
49 X. W. Lou, D. Deng, J. Y. Lee, J. Feng and L. A. Archer, *Adv. Mater.*, 2008, **20**, 258.
50 X. Wang, H. Guan, S. Chen, H. Li, T. Zhai, D. Tang, Y. Bando and D. Golberg, *Chem. Commun.*, 2011, **47**, 12280.
51 X. Wang, X.-L. Wu, Y.-G. Guo, Y. Zhong, X. Cao, Y. Ma and J. Yao, *Adv. Funct. Mater.*, 2010, **20**, 1680.
52 S. H. Lee, S.-H. Yu, J. E. Lee, A. Jin, D. J. Lee, N. Lee, H. Jo, K. Shin, T.-Y. Ahn, Y.-W. Kim, H. Choe, Y.-E. Sung and T. Hyeon, *Nano Lett.*, 2013, **13**, 4249.
53 Q. Guan, J. L. Cheng, X. D. Li, B. Wang, L. Huang, F. D. Nie and W. Ni, *Sci. Rep.*, 2015, **5**, 10017.